Geophysical Research Letters

RESEARCH LETTER
10.1029/2022GL101211

Northern Hemisphere Heat Extremes in a Warmer Climate: More Probable but Less Colocated With Blocking

V. Narinesingh[1,2], J. F. Booth[3], and Y. Ming[4]

[1]NOAA Geophysical Fluid Dynamics Laboratory, Princeton, NJ, USA, [2]Program in Atmospheric and Oceanic Sciences, Princeton University, Princeton, NJ, USA, [3]Earth and Atmospheric Sciences, City University of New York—City College, New York, NY, USA, [4]Department of Earth and Environmental Sciences, Boston College, Boston, MA, USA

Key Points:

- Blocking is more colocated with heat extremes over land than ocean. Stronger heat extremes are more colocated with blocking
- End of 20th century 90th percentile temperatures become 0–70th percentile by the end of the 21st century in a high emissions scenario
- Land heat extreme duration is unchanged in RCP 8.5, but colocated blocking decreases, suggesting changes in dynamics driving heat extremes

Supporting Information:

Supporting Information may be found in the online version of this article.

Correspondence to:

V. Narinesingh,
VeeNarinesingh@gmail.com

Citation:

Narinesingh, V., Booth, J. F., & Ming, Y. (2023). Northern Hemisphere heat extremes in a warmer climate: More probable but less colocated with blocking. *Geophysical Research Letters*, *50*, e2022GL101211. https://doi.org/10.1029/2022GL101211

Received 8 SEP 2022
Accepted 1 JAN 2023

Author Contributions:

Conceptualization: V. Narinesingh, J. F. Booth, Y. Ming
Data curation: Y. Ming
Formal analysis: V. Narinesingh
Funding acquisition: J. F. Booth
Investigation: V. Narinesingh
Methodology: V. Narinesingh, J. F. Booth
Supervision: J. F. Booth, Y. Ming
Validation: V. Narinesingh
Visualization: V. Narinesingh
Writing – original draft: V. Narinesingh, J. F. Booth

Abstract This work uses reanalysis and NOAA Geophysical Fluid Dynamics Laboratory's Coupled Model Intercomparison Project 6 model, CM4, to investigate the colocation of heat extremes and atmospheric blocking in the current climate and an end of 21st century, extreme-emissions projection. In the present day, the colocation of heat events and blocking is greatest for the strongest heat events. Block-heat extreme colocation is found to be less prevalent over ocean than land, exhibiting regional variation throughout the Northern Hemisphere. Over North America, colocation is greatest near the northwestern and northeastern coasts, minimizing near the center; over Eurasia, colocation is most prevalent in northern regions. In an RCP 8.5 projection, the historical 90th percentile temperature decreases to 0–70th percentile, depending on the region. This is primarily driven by mean state warming. Blocking is found to decrease along with the colocation of blocking and heat extremes, suggesting that in some regions, the mechanisms driving heat extremes will change in future climates.

Plain Language Summary This work investigates extreme heat events and atmospheric blocks (persistent high-pressure systems), which are known to be strongly linked. The analysis herein shows that the strongest extreme heat events coincide with atmospheric blocks, however, the likelihood of the events being colocated varies from region to region. In a high emissions warming scenario, temperatures exceeding the warmest 10% in the current climate, occur 30%–100% of the time depending on the region. This is mostly driven by an increase in average temperature everywhere—rather than an increase in the variability of the temperature. At the same time, the model predicts that blocking, and the colocation of extremes heat events with blocking, decreases, suggesting the physical drivers of heat extremes will change in a warmer climate.

1. Introduction

Persistent heat extremes can have devastating impacts on ecosystems and society (Garcia-Herrera et al., 2010; Shaposhnikov et al., 2014; Wegren, 2011). Thus, it is of great importance to understand the dynamics of these events and how they might evolve in warmer climates (Horton et al., 2016; Perkins, 2015). In this article the relationship between heat extremes and atmospheric blocking is examined –both in the current climate and in an extreme emissions (Hausfather & Peters, 2020) climate model projection of the end of the 21st century.

Atmospheric blocks are large (~10^6 km^2), persistent (5+ days), quasi-stationary anticyclones (Lupo, 2021; Rex, 1950) linked to hazardous weather phenomena. In particular, case studies and global statistical analyses have found that blocks can be drivers of persistent heat extremes (Chan et al., 2019, 2022; Pfahl & Wernli, 2012; Suarez-Gutierrez et al., 2020; Trenberth & Fasullo, 2012). When colocated with heat extremes, blocked flow can generate warmer temperatures through (a) adiabatic compression of subsiding air, and (b) diabatic heating effects induced by clear skies (i.e., drying of soil moisture, greater sensible heat flux; e.g., Horton et al., 2016); When offset with heat extremes, blocking can also drive temperatures via warm horizontal advection (Pfahl, 2014).

The dominating mechanisms to which blocks drive heat extremes has been found to be regionally dependent (Brunner et al., 2018; Pfahl, 2014; Pfahl & Wernli, 2012). For example, northern European heat extremes tend to be more colocated with blocking, whereas southern European events tend to be more offset (Pfahl, 2014). In recent work, Chan et al. (2022) analyzed blocking and heat waves focusing on Euro-Atlantic regions and area-averages over the entire Northern Hemisphere (NH) extratropics. Herein, we complement that work with a gridpoint-by-gridpoint probabilistic analysis of the colocation of blocking occurrence and extreme heat events

Writing – review & editing: V. Narinesingh, J. F. Booth, Y. Ming

throughout the NH extratropics. To do this, we investigate the colocation of blocking and heat extremes in the NH—both in current and future possible climates.

On one hand, heat extremes are projected to increase in future climates (Collins et al., 2014; Fischer & Knutti, 2015); On the other hand, blocking is projected to decrease (Chan et al., 2022; Davini & D'Andrea, 2020; Woolings et al., 2018). This then begs the questions: In a warmer climate, does blocking play a less prevalent role in driving heat extremes? If so, do the changes have specific regional variability, and will the duration of extremes change as well? This paper aims to address these questions as well as document the regional variability of the colocation of blocking and heat extremes in the current climate.

2. Materials and Methods

2.1. Reanalysis and General Circulation Models

We focus on NH summer defined as the months of June, July, and August. First, ERA5 reanalysis (Hersbach et al., 2020) is used to analyze the colocation of atmospheric blocking and persistent heat extremes from 1980 to 2014.

Then, the colocation of atmospheric blocking and persistent heat events in a comprehensive general circulation model is analyzed. For this, the Geophysical Fluid Dynamics Laboratory's (GFDL) coupled atmosphere-ocean model, CM4 (Held et al., 2019), is used. CM4 is part of the Coupled Model Intercomparison Project 6 (CMIP6; Eyring et al., 2016). CM4 consists of the GFDL atmosphere model AM4 (Zhao et al., 2018) coupled to the GFDL ocean model OM4 (Adcroft et al., 2019). The atmosphere is integrated at roughly 100-km horizontal resolution on 33 vertical levels.

Two separate climate simulations are analyzed, one historical and one climate projection. The first climate simulation is a historical integration that includes time-evolving solar irradiance, aerosol precursor emissions, and green-house gas concentrations. These features provide realistic forcing conditions and follow CMIP specifications. The model period spanning 1980–2014 is analyzed and referred to herein as the historical integration of CM4 or "Hist."

To investigate the effects of anthropogenic climate change on blocking and heat extremes, a representative concentration pathway 8.5 (RCP 8.5; Riahi et al., 2011) simulation of CM4 is analyzed. RCP 8.5 assumes a continued rise of greenhouse gas emissions throughout the 21st century. RCP 8.5 leads to a radiative forcing of 8.5 W m^{-2} by the year 2100. Though this scenario might be unrealistic (Hausfather & Peters, 2020), it is still useful in demonstrating physical responses to warming. The analyses in this paper focus on the projection for years 2065–2099.

For all analyses in this article daily mean data on 2.0 × 2.5 latitude by longitude grids are used. This resolution was chosen due to what was the most readily accessible geopotential height data from the CM4 integrations. Although ERA5 data is available at finer resolution, we chose to use ERA5 data on 2.0 × 2.5-degree grids to avoid numerical errors if we instead interpolated the CM4 data onto finer grids. The chosen resolution yields blocking climatologies and properties consistent with previous studies (Dunn-Sigouin & Son, 2013; Narinesingh et al., 2022; e.g., Woolings et al., 2018 and the references therein).

2.2. Block Tracking and Climatology

To identify and track summer blocking, the methodology of Chan et al. (2019) is implemented. This metric is a modification of the 500 hPa geopotential height (Z_{500}) metric in Dunn-Sigouin and Son (2013). Both versions are hybrid metrics, meaning they search for contiguous, positive, high amplitude Z_{500} anomalies that also reverse the meridional gradient of Z_{500}. The modification in Chan et al. (2019), however, is better for summer blocking, where both the anomaly amplitude and area thresholds are reduced compared to Dunn-Sigouin and Son (2013). Full details of the block tracking algorithm can be found in the Supporting Information S1 section.

To calculate the climatology of blocking, $P(B)$, for each timestep, the block tracking algorithm yields binary lat-lon grids where ones indicate blocked gridpoints, while zeroes denote no blocking is present. These grids are then averaged over all summer timesteps (June, July, August) to yield $P(B)$ (Figure 1). $P(B)$ is the percentage

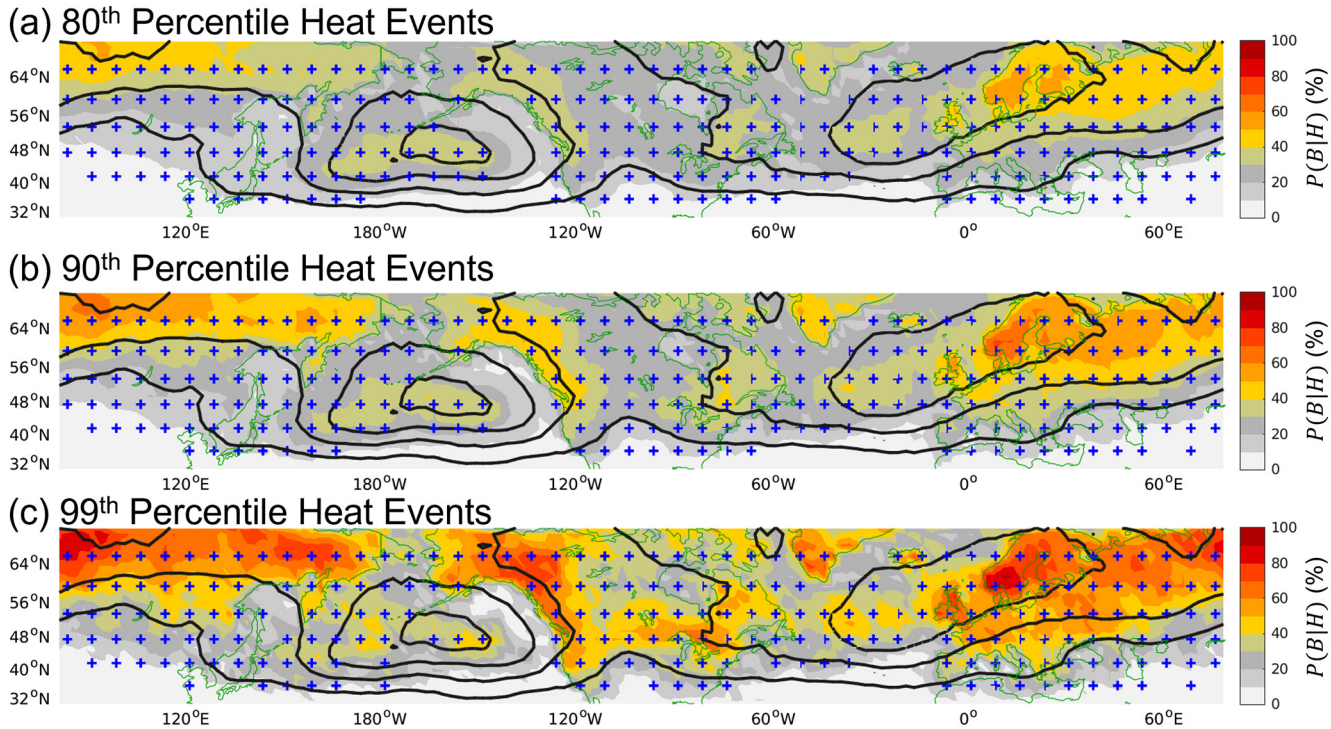

Figure 1. In ERA 5 reanalysis, percent of extreme heat event days on which blocking is colocated with the event (shading), $P(B|H)$, for (a) 80th, (b) 90th, and (c) 99th percentile events. Contours indicate the percent of all summer days that are blocked, $P(B)$. The outer contour and contour interval is 5%. Blue stippling indicates significant differences between $P(B|H)$ and $P(B)$.

of days that a block is present out of all summer days. For example, regions of $P(B) = 20\%$ corresponds to 644 blocked days out of 3220 total summer days in the 35-year dataset.

2.3. Persistent Extreme Heat Events: Tracking and Block Association

The persistent heat extreme metric described in Chan et al. (2019) is used for the analyses herein. First, a 5-day running mean is applied to daily maximum 2-m temperature data, T, yielding the smoothed field $\tilde{T}$ (Equation 1). This time-averaging approach filters the temperature field to emphasize persistent events with timescales comparable to blocking (Chan et al., 2019). Then, a 29-day by 11-year running mean, $\hat{T}$ (Equation 2), is subtracted to remove the seasonal cycle and long-term trend. Note, $\hat{T}$ and $\tilde{T}$ are functions of day, d, and can also be written as a function of the corresponding year, y. Subtracting $\hat{T}$ from $\tilde{T}$ yields the 2 m temperature anomaly field, T' (Equation 3). At the data endpoints, all running averages use the data that is available when there are fewer elements than the window size.

$$\tilde{T}(d,y) = \frac{1}{5}\sum_{\delta=d-2}^{d+2} T(\delta) \tag{1}$$

$$\hat{T}(d,y) = \frac{1}{11}\sum_{\upsilon=y-5}^{y+5}\frac{1}{29}\sum_{\delta=d-14}^{d+14}\tilde{T}(\delta,\upsilon) \tag{2}$$

$$T'(d,y) = \tilde{T} - \hat{T} \tag{3}$$

For the analyses in this paper, persistent heat extremes of increasing magnitude are examined by identifying timesteps with temperature anomalies exceeding the 80th, 90th, and 99th percentiles. For each magnitude of intensity, the conditional probability, $P(B|H)$, is calculated at each grid-cell. $P(B|H)$ is defined as the following: given a persistent heat extreme, the probability of blocking being colocated in the same gridcell (Figure 1). By definition, the climatological frequency of 80th, 90th, and 99th percentile persistent heat extremes are 20%,

10%, and 1% everywhere, respectively. Full details for the significance calculations are located in the Supporting Information S1.

3. Results

3.1. The Association of Blocking and Heat Extremes in Reanalysis

For this analysis, we will report the results by continental region. Blocking occurs approximately 5%–10% of summer days over most of North America (Figure 1). During heat extremes, however, blocking frequency increases significantly. During 90th percentile heat extremes, the frequency of blocking increases to 20%–30% over central North America and to 30%–50% near the northeastern and northwestern coasts (Figure 1b); For 99th percentile extreme heat events, blocking frequency increases to 30%–50% and 40%–80%, respectively (Figure 1c). In southern Eurasia, blocking frequency ranges from 5% to 10%, and in Northern Eurasia, blocking occurs 10%–20%. During 90th percentile heat events, however, blocking frequency jumps to 30%–70% throughout the continent. For 99th percentile events these frequencies increase by an additional 10%–20%.

Over land, increased heat extreme severity is associated with a greater probability of events being colocated with blocking (Figures 1a–1c). A regional variation in the colocation of blocking and heat extremes is also evident. In North America, the frequency of heat extremes colocated with blocks maximizes in the northwestern (NW) and northeastern (NE) parts of the continent (Figure 1c). In Europe, the colocation of blocking and heat extremes is most frequent over northern Europe and less frequent equatorward; This agrees with Pfahl (2014), who found that southern European heat extremes tend to be more driven by horizontal advection, matching the lack of colocated blocking in the region that we show in Figure 1.

Over the ocean, the colocation of blocking and heat extremes is not as prevalent as over land: $P(B|H)$ has values of 70%–90% over some land areas, but never reaches above 60% over the ocean. The contrast in block-heat extreme colocation over land versus ocean highlights the distinct mechanisms that can drive heat extremes over the two surfaces –including ocean advection and heat flux convergence (Oliver et al., 2021).

3.2. Blocking and Heat Extreme Simulation in CM4

The GFDL global climate model, CM4, is able to reproduce the spatial structure of the blocking climatology found in reanalysis (Figure 2). The blocking climatology features a bimodal spatial distribution with maxima near Alaska and Greenland, consistent with previous findings (e.g., Woollings et al., 2018). No significant blocking biases over North America and Northern Eurasia occur in CM4. However, near southern Europe and extending eastward into the western Pacific there is more blocking in the model than reanalysis.

Figures 2b and 2c shows the percentage of extreme heat events that are colocated with blocking. The model demonstrates similar event association compared to reanalysis. CM4 captures the properties that: (a) as the severity of heat threshold is raised, more heat events are colocated with blocking—that is, it captures a positive relationship in $P(B|H)$ with respect to increased heat extreme threshold, and (b), more heat events over land are colocated with blocking as compared to over the ocean. The regional variation in heat extreme and blocking colocation is also captured by CM4 (Figures 1, 2b, and 2c). For example, the northeastern and northwestern coasts of North America have greater colocation of heat extremes and blocking compared to central parts of the continent. In addition, CM4 also simulates that heat extremes over Scandinavia are most colocated with blocking compared to the rest of Eurasia.

Overall, CM4 reproduces the frequency of blocking over North America and northern Eurasia but deviates for southern Eurasia. Nonetheless, CM4 produces a similar association of heat extremes with atmospheric blocking compared to reanalysis. Next, we investigate the model's simulation of blocking and heat extremes in the RCP 8.5 climate scenario.

3.3. End of 21st Century in RCP 8.5: Historical 90th Percentile Versus Mean State Warming

For our analysis of model output from the forced climate simulation, the first question we address is: How does the 90th percentile temperature anomaly in the historical climate compare to the magnitude of mean state warming in the RCP 8.5 simulation?

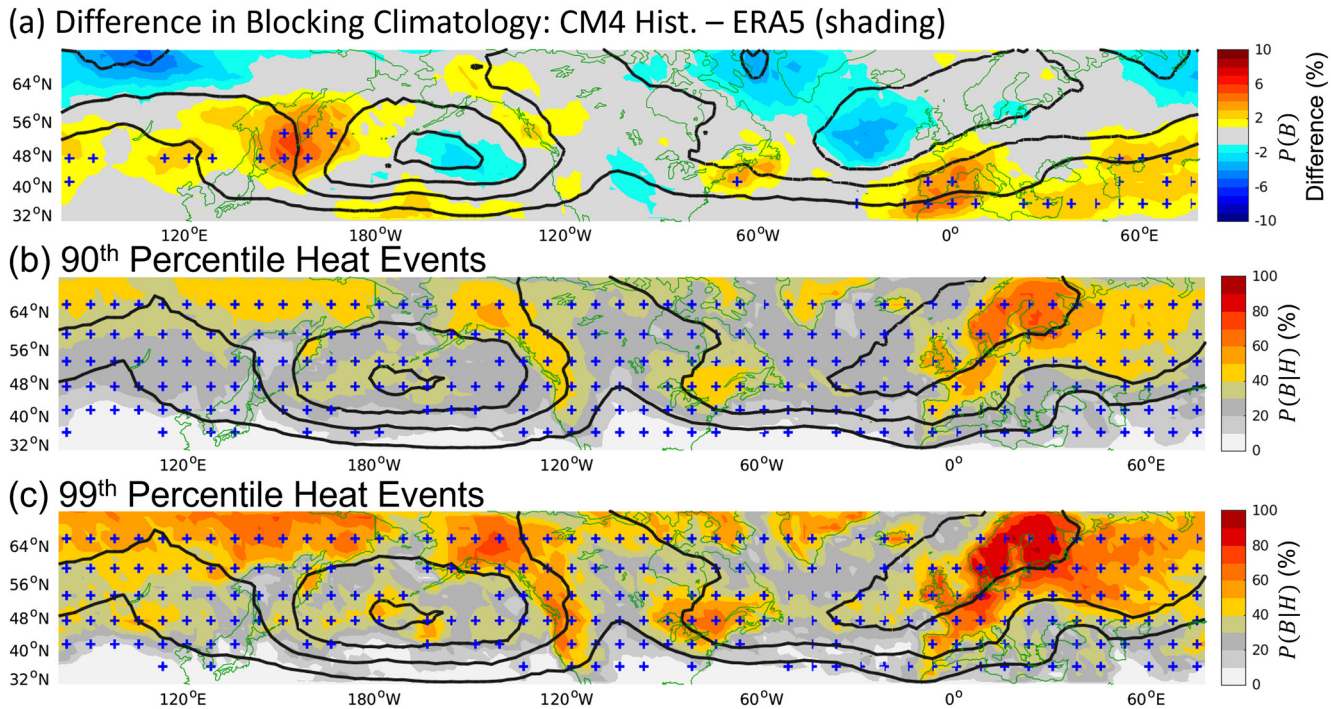

Figure 2. (a) Difference in blocking climatology, $P(B)$, CM4 historical minus ERA5 reanalysis (shading). $P(B)$ in ERA5 reanalysis is shown in contours with outer contour and contour interval of 5%. (b, c) In CM4's historical integration, percent of extreme heat event days that include blocking (shading), $P(B|H)$, for (b) 90th and (c) 99th percentile events. $P(B)$ in CM4 Hist. is shown in contours. Blue stippling indicates significant differences between (a) $P(B)$ between ERA5 and CM4 Hist., and (b, c) $P(B|H)$ and $P(B)$ in CM4. Hist. for 90th and 99th percentile heat events, respectively.

Figure 3a shows the difference in the summer surface temperature climatology between the RCP 8.5 and historical CM4 integrations; Figure 3b shows the 90th percentile anomaly used to define extreme heat events in the historical integration, $T_{90\text{th Hist.}}$; Figure 3c then shows the difference between the two. Throughout most of the NH midlatitudes, RCP 8.5 mean state warming exceeds $T_{90\text{th Hist.}}$ (Figure 3c).

Consistent with this mean state warming, and other climate projection studies (e.g., Horton et al., 2016), temperatures exceeding the 90th percentile of the historical climate occur more often in RCP 8.5. To deduce this, we calculate temperature anomalies in RCP 8.5, $T'^{*}_{\text{RCP 8.5}}$, with respect to the historical climate, inherently including the mean-state warming between the integrations. Specifically, $T'^{*}_{\text{RCP 8.5}}$ (Equation 4) is calculated by subtracting the mean state of the historical integration, $\hat{T}_{\text{Hist.}}$, from the time-filtered surface temperature field in RCP 8.5, $\tilde{T}_{\text{RCP 8.5}}$ (as defined in Equation 1).

$$T'^{*}_{\text{RCP 8.5}} = \tilde{T}_{\text{RCP 8.5}} - \hat{T}_{\text{Hist.}} \tag{4}$$

Then, at each gridpoint, $T_{90\text{th Hist.}}$ (Figure 3b) is compared to distributions of $T'^{*}_{\text{RCP 8.5}}$, determining how $T_{90\text{th Hist.}}$ ranks amongst events in RCP 8.5 (Figure 3d).

Over midlatitude oceans, $T_{90\text{th Hist.}}$ is now between the 0–5th percentile in RCP 8.5. This means that in RCP 8.5 temperatures exceed the 90th percentile in the historical climate nearly all of the time. The one exception to this is in the North Atlantic, where $T_{90\text{th Hist.}}$ corresponds to only the 30–35th percentile in RCP 8.5, consistent with this region being where mean-state warming minimizes (Figure 3a). Still, for most of the ocean, future temperatures are projected to exceed the historical 90th percentile temperature all of the time (Figure 3d). Part of this is due to the small range of variability in ocean surface temperatures in the current climate, however, the fact remains that the mean state warming exceeds present day variability for these regions.

Over land, there is some regional variation in the rank of the historical 90th percentile in the RCP 8.5 climate (Figure 3d): (a) central North America drops to the 30–50th percentile while the rest of the continent mostly sees a drop to the 0–30th percentile. (b) In western and northern Europe, there is a drop to 0–40th percentile

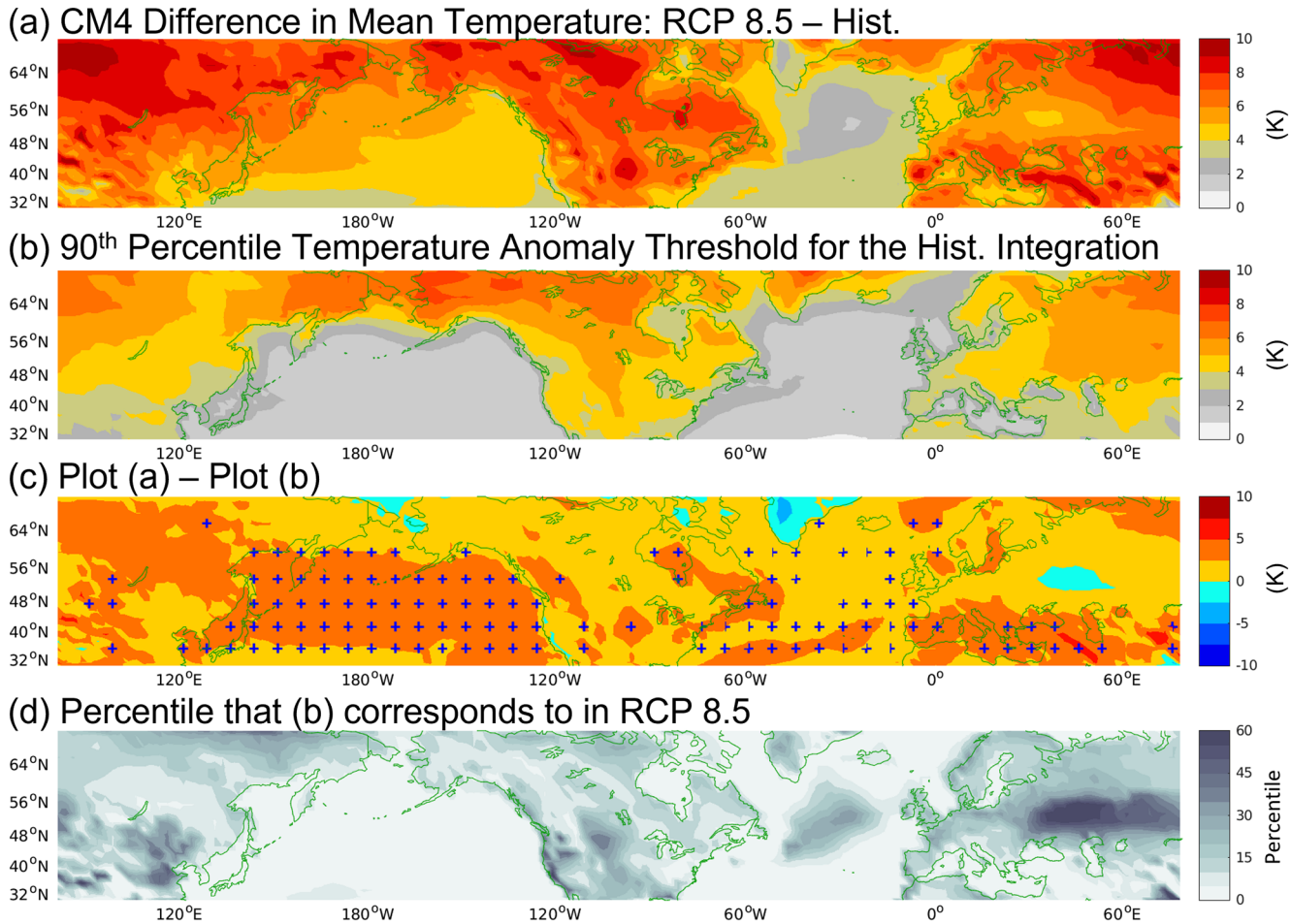

Figure 3. (a) Difference in summer mean surface temperatures in RCP 8.5 and the historical CM4 integrations. (b) Anomaly threshold for 90th percentile extreme heat events in the CM4 historical integration. (c) Difference between plots (a, b). Blue stippling denotes significant differences. (d) The percentile that (b) corresponds to in RCP 8.5.

but over the Eurasian Steppe only 50–60th. Still, all places over land show a drop to 60th percentile or lower. In other words, what was once considered the minimum for the top 10% of temperatures in the historical climate, becomes closer to the norm in the RCP 8.5 projection. This increased occurrence of temperatures exceeding the historical 90th percentile can be interpreted as a shift of the entire distribution (not shown) to warmer temperatures –leading to a much warmer climatology (Figure 3a), which is consistent with previous findings (Schneider et al., 2015).

3.4. RCP 8.5 Heat Extremes: Changes in Block Colocation and Heat Extreme Duration

3.4.1. Blocking Climatology and Block-Heat Extreme Colocation

Next, we use the RCP 8.5 integration to examine atmospheric blocking and the colocation of heat extremes in a warmer world. In observations and CM4's historical simulation, we saw the strongest heat events had increased likelihood to be colocated with blocking (Figures 1 and 2). As such, we now turn our attention to the strongest events in the warmer, RCP 8.5 climate.

In this case, because our focus is on circulation and temperature anomalies, we now switch to define our RCP 8.5 heat extremes using anomalies, $T'_{\text{RCP 8.5}}$ (Equation 5), with respect to the RCP 8.5 mean state, $\hat{T}_{\text{RCP 8.5.}}$.

$$T'_{\text{RCP 8.5}} = \tilde{T}_{\text{RCP 8.5}} - \hat{T}_{\text{RCP 8.5.}} \tag{5}$$

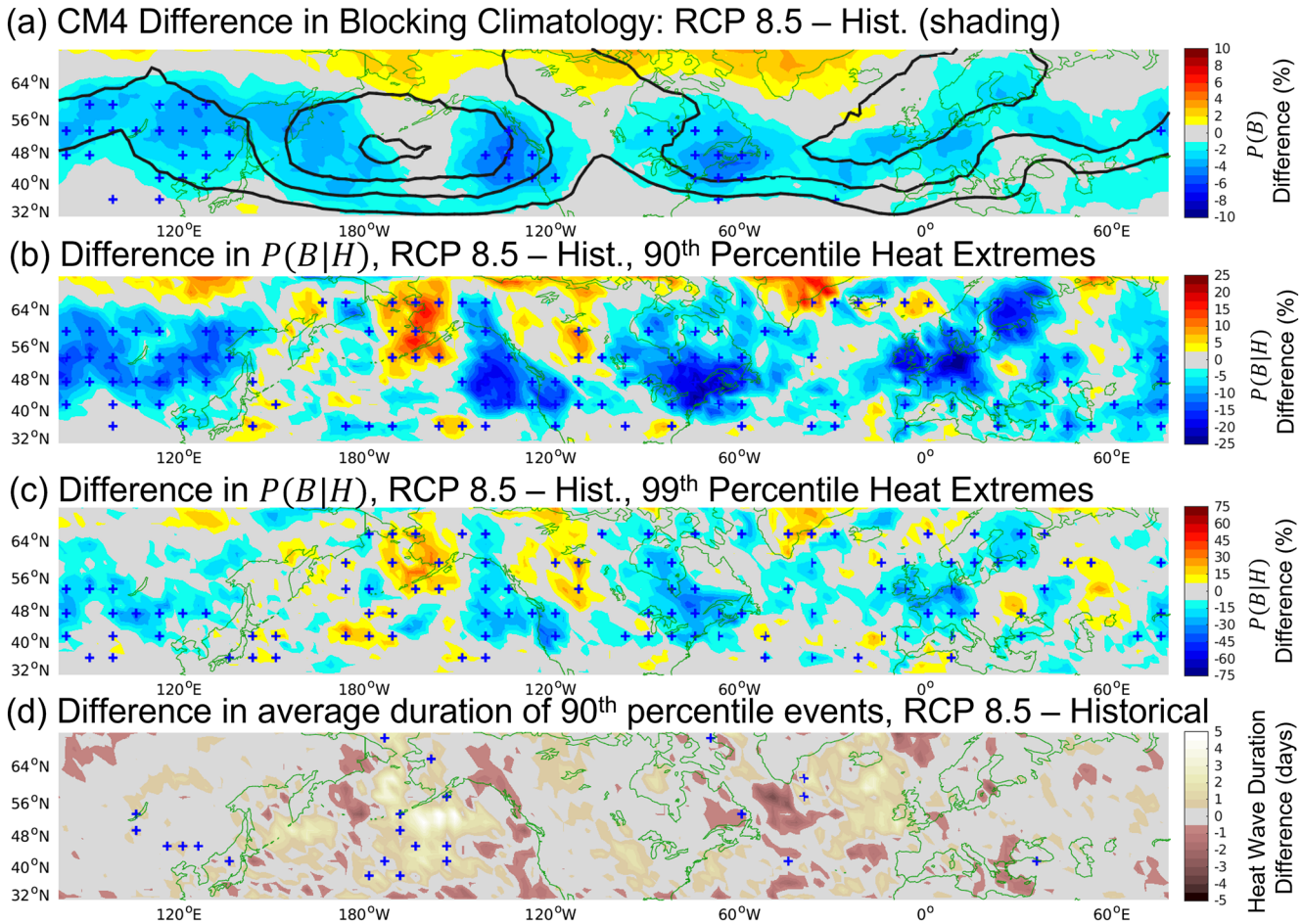

Figure 4. (a) Difference in the blocking climatology, $P(B)$, for CM4 RCP 8.5 minus CM4 historical (shading). $P(B)$ in CM4 historical (contours). Outer contour and contour interval is 5%. (b, c) Difference in percent of heat extreme days that include blocking, $P(B|H)$, CM4 RCP 8.5 subtracting CM4 historical (shading) for (b) 90th and (c) 99th percentile heat events. (d) Difference in average duration of 90th percentile heat events in RCP 8.5 and the historical integration. Blue stippling denotes significant differences between the quantities being compared in each panel. Note, there is a difference in color axes between (b, c).

This allows to us to make a comparison between the occurrence of blocking during heat extremes in two different climates. We note, blocking is also defined with respect to a climatology, and we use historical and RCP 8.5 climatologies to define the historical and RCP 8.5 blocks, respectively.

Blocking is found to decrease throughout the hemisphere (Figure 4a), consistent with previous findings (Chan et al., 2022, e.g., Woollings et al., 2018). The regions in which decreased blocking are statistically significant are near the western and eastern coasts of North America, as well as eastern Asia –regions where blocking occurs nearly half as frequently in the last 35 years of the 21st century. Decreases in blocking are found to be robust to changes in the criteria used in the identification algorithm, such as: removing the block tracking criteria of a gradient reversal; and, separately, increasing anomaly and area thresholds as in Dunn-Sigouin and Son (2013).

As with blocking itself (Figure 4a), the colocation of blocking and persistent heat extremes decreases in RCP 8.5 (Figures 4b and 4c). We find that regions of decreased block-heat extreme colocation correspond to regions of significant reduction in blocking (Figure 4a). For 90th percentile events, colocation with blocking decreases 10%–30% (Figure 4b); For 99th percentile events, colocation is reduced by 20%–40% (Figure 4c). Thus, $P(B|H)$ in RCP 8.5 becomes nearly half as probable as in the historical climate (Figures 2b and 2c). This is consistent with the findings of Chan. et al. (2022), who found heat extremes over land in RCP 8.5 to be less correlated with blocking across CMIP6 models. Together, our findings along with Chan et al. (2022) suggests that at the synoptic scale of the atmosphere (~1,000 km), the physical mechanisms important for persistent heat extremes in RCP 8.5 differ from the historical climate.

3.4.2. 90th Percentile Heat Extreme Duration

To get a sense of how heat extremes may change as a result of decreased colocated blocking, heat extreme duration is examined. At each grid point heat extremes are grouped into separate continuous events. Heat extreme duration is classified as the number of successive days in which the temperature anomaly exceeds the 90th percentile. Note, the 5-day running mean at the beginning of the anomaly calculation smooths out any 1–3-day spikes or dips in the 2-m temperature field. Then, the average duration of all heat extremes at a gridpoint is calculated. Figure S1 in Supporting Information S1 shows average duration at each grid point for each model.

Over land, with the exception of a few places in East Asia, no significant differences in 90th percentile heat extreme duration are found between RCP 8.5 and Hist. (Figure 4d). This is despite decreases in colocated blocking (Figures 4a and 4b). Though there is some suggestion that heat extreme duration increases over midwestern North America, these changes are insignificant by the standards set here.

On the other hand, over ocean, heat extreme duration does change in certain regions. Over the north Pacific and parts of the north Atlantic basins, there are significant increases in duration even though blocking generally decreases in this regions.

Taken together, the results over land and ocean suggest that the colocation of blocking does not have a strong control on heat extreme duration in RCP 8.5. In addition, it is important to note that although 90th percentile heat extremes over land in RCP 8.5 are generally not more persistent than in the historical climate, events that would be considered extreme in the historical climate now become the norm in RCP 8.5 (as discussed with Figure 3).

4. Discussion and Conclusions

In this analysis, the colocation of persistent heat extremes and atmospheric blocking is investigated for the current climate and a high-emissions, end of 21st century projection. Focusing first on the current climate, it is found that the stronger heat extreme, the higher the likelihood of it being colocated with blocking (Figure 1), and the colocation of heat extremes and blocking shows strong regional variation: (a) In North America, event colocation maximizes in the northeastern and northwestern parts of the continent, and minimizes near the center (Figure 1), (b) In Eurasia, event colocation is greater in the northern sectors of the landmass compared to the south.

These findings in Eurasia agree with Pfahl (2014), who finds that over northern Europe, heat extremes tend to be more colocated with blocking and thus are more likely to be maintained by subsidence and radiative effects; While over southern Europe, heat extremes are associated with warm horizontal advection induced by strong anticyclonic flow to the northeast.

Taken together, our results and Pfahl's work suggest that over northeastern and northwestern North America, where block-heat extreme colocation is most prevalent (Figure 1), subsidence and radiative effects could be the key drivers of heat extremes. Furthermore, over central North America, where block-heat extreme colocation minimizes, events may be more driven by horizontal advection or other effects. To further investigate this, future work could examine the advective and diabatic terms of the near-surface temperature tendency (a technique explored in Nabizadeh et al., 2021) from region to region. This would be especially helpful for North America, which is much less studied compared to Europe.

In reanalysis data, we also find that block-heat extreme colocation is more prevalent over land than it is over ocean. This result emphasizes the fact that over the ocean, ocean circulation also plays an important role in generating heat events –in addition to the atmosphere (e.g., Oliver et al., 2021). For example, although blocking circulation can create conditions conducive to strong sensible and shortwave heat fluxes into the ocean, ocean circulation can counteract this via anomalous horizontal advection or upwelling of colder water. Furthermore, over land net cooling reduction from soil moisture depletion plays a role not found over ocean.

We then go on to examine heat extremes and blocking in NOAA GFDL's CM4 for a historical simulation and an end of 21st century climate projection (RCP 8.5). In the historical simulation, CM4 captures the regional variation in block and heat extreme colocation, as well as increased colocation for more severe extremes (Figure 2). This agreement shows that the model reproduces the various atmospheric circulation patterns that drive heat extremes throughout different regions, as well as the subsequent anomalous temperatures.

In the RCP 8.5 projection, temperatures exceeding the historical 90th percentile threshold are much more prevalent: over land the historical 90th percentile temperature becomes 0–60th percentile and 0–30th percentile over

ocean (Figure 3d). This means that by the end of the RCP 8.5 21st century, temperatures in the top 10% of all summer days in the historical climate, now occur regularly, around 30%–100% of the time, everywhere. This increased probability of warm events is primarily due to changes in the mean state temperature rather than changes in synoptic scale dynamics, consistent with previous findings (Chan et al., 2022; Schneider et al., 2015). We also note that the magnitude of increased likelihood varies from region to region, perhaps indicative of circulation changes.

On the other hand, blocking is projected to decrease, as is the colocation of blocking and heat extremes. This is consistent with recent findings by Chan et al., 2022, who also found less blocking and block-heat extreme association, but increased heatwave occurrence driven primarily by mean state warming. Decreases in block-heat extreme colocation could point to changes in the dominating mechanical and thermodynamic drivers of persistent heat extremes in a warmer world. For example, where more colocated events were driven by clear sky diabatic effects and warming via the compression of subsiding air, perhaps in the future, warm horizontal advection could play a more major role when blocks are not as colocated (Pfahl, 2014).

One could argue that in a warmer world, the decrease in blocking could actually be a benefit because the circulation patterns that typically drive persistent heat extremes occur less often. However, we find that this decrease does not matter. In this high-emissions scenario the duration of extreme heat events remains mostly unchanged over land (Figure 4d), and the mean state temperature becomes so much warmer that temperatures that were once considered extreme in the historical climate, now become close to average in RCP 8.5 –regardless of blocking circulation.

That being said, it is important to note that RCP 8.5 might be a worst-possible case for a forcing scenario (Hausfather & Peters, 2020) and open questions still remain on whether or not warming simulations accurately capture changes in the physical properties of blocking (e.g., Woollings et al., 2018). Still, the present study is useful in understanding the response of blocking and heat extremes to a warmer climate in general, and also discerning signal to noise in similar experiments utilizing more realistic end of 21st century forcing.

Data Availability Statement

ERA5 reanalysis data can be downloaded from the European Center for Medium Range Weather Forecasts (https://www.ecmwf.int/en/forecasts/datasets/reanalysis-datasets/era5). Data from GFDL CM4 can be downloaded from The World Climate Research Programma Coupled Model Intercomparison Project 6 webpage (https://esgf-node.llnl.gov/search/cmip6/).

Acknowledgments
This publication was supported through NOAA Educational Partnership Program/Minority-Serving Institutions award number NA16SEC4810008 to the Center for Earth System Sciences and Remote Sensing Technologies at The City College of New York. The authors thank The City College of New York, NOAA Center for Earth System Sciences and Remote Sensing Technologies, and the NOAA Office of Education, Educational Partnership Program for fellowship support for Veeshan Narinesingh. Contents are solely the responsibility of the award recipient and may not represent official views of NOAA or the U.S. Department of Commerce.

References

Adcroft, A., Anderson, W., Balaji, V., Blanton, C., Bushuk, M., Dufour, C. O., et al. (2019). The GFDL global ocean and sea ice model OM4.0: Model description and simulation features. *Journal of Advances in Modeling Earth Systems*, *11*(10), 3167–3211. https://doi.org/10.1029/2019MS001726

Brunner, L., Schaller, N., Anstey, J., Sillmann, J., & Steiner, A. K. (2018). Dependence of present and future European temperature extremes on the location of atmospheric blocking. *Geophysical Research Letters*, *45*(12), 6311–6320. https://doi.org/10.1029/2018GL077837

Chan, P., Hassanzadeh, P., & Kuang, Z. (2019). Evaluating indices of blocking anticyclones in terms of their linear relations with surface hot extremes. *Geophysical Research Letters*, *46*(9), 4904–4912. https://doi.org/10.1029/2019GL083307

Chan, P. W., Catto, J. L., & Collins, M. (2022). Heatwave–blocking relation change likely dominates over decrease in blocking frequency under global warming. *NPJ climate and atmospheric science*, *5*(1), 1–8. https://doi.org/10.1038/s41612-022-00290-2

Collins, M., Knutti, R., Arblaster, J. M., Dufresne, J., Fichefet, T., Friedlingstein, P., et al. (2014). *Long-term Climate Change: Projections, Commitments and Irreversibility*, In Anonymous (Ed.), Cambridge University Press.

Davini, P., & D'Andrea, F. (2020). From CMIP3 to CMIP6: Northern Hemisphere atmospheric blocking simulation in present and future climate. *Journal of Climate*, *33*(23), 10021–10038. https://doi.org/10.1175/JCLI-D-19-0862.1

Dunn-Sigouin, E., & Son, S. (2013). Northern Hemisphere blocking frequency and duration in the CMIP5 models. *Journal of Geophysical Research: Atmospheres*, *118*(3), 1179–1188. https://doi.org/10.1002/jgrd.50143

Eyring, V., Bony, S., Meehl, G. A., Senior, C. A., Stevens, B., Stouffer, R. J., & Taylor, K. E. (2016). Overview of the Coupled Model Intercomparison Project Phase 6 (CMIP6) experimental design and organization. *Geoscientific Model Development*, *9*(5), 1937–1958. https://doi.org/10.5194/gmd-9-1937-2016

Fischer, E. M., & Knutti, R. (2015). Anthropogenic contribution to global occurrence of heavy-precipitation and high-temperature extremes. *Nature Climate Change*, *5*(6), 560–564. https://doi.org/10.1038/nclimate2617

García-Herrera, R., Díaz, J., Trigo, R. M., Luterbacher, J., & Fischer, E. M. (2010). A review of the European summer heat wave of 2003. *Critical Reviews in Environmental Science and Technology*, *40*(4), 267–306. https://doi.org/10.1080/10643380802238137

Hausfather, Z., & Peters, G. P. (2020). Emissions—The "business as usual" story is misleading. *Nature (London)*, *577*(7792), 618–620. https://doi.org/10.1038/d41586-020-00177-3

Held, I. M., Guo, H., Adcroft, A., Dunne, J. P., Horowitz, L. W., Krasting, J., et al. (2019). Structure and performance of GFDL's CM4.0 climate model. *Journal of Advances in Modeling Earth Systems*, *11*(11), 3691–3727. https://doi.org/10.1029/2019MS001829

Hersbach, H., Bell, B., Berrisford, P., Hirahara, S., Horányi, A., Muñoz-Sabater, J., et al. (2020). The ERA5 global reanalysis. *Quarterly Journal of the Royal Meteorological Society*, *146*(730), 1999–2049. https://doi.org/10.1002/qj.3803

Horton, R. M., Mankin, J. S., Lesk, C., Coffel, E., & Raymond, C. (2016). A review of recent advances in research on extreme heat events. *Current Climate Change Reports*, *2*(4), 242–259. https://doi.org/10.1007/s40641-016-0042-x

Lupo, A. R. (2021). Atmospheric blocking events: A review. *Annals of the New York Academy of Sciences*, *1504*(1), 5–24. https://doi.org/10.1111/nyas.14557

Nabizadeh, E., Lubis, S. W., & Hassanzadeh, P. (2021). The 3D structure of northern hemisphere blocking events: Climatology, role of moisture, and response to climate change. *Journal of Climate*, *34*(24), 1–54. https://doi.org/10.1175/JCLI-D-21-0141.1

Narinesingh, V., Booth, J. F., & Ming, Y. (2022). Blocking and general circulation in GFDL comprehensive climate models. *Journal of Climate*, *35*(12), 3687–3703. https://doi.org/10.1175/JCLI-D-21-0486.1

Oliver, E. C. J., Benthuysen, J. A., Darmaraki, S., Donat, M. G., Hobday, A. J., Holbrook, N. J., et al. (2021). Marine heatwaves. *Annual Review of Marine Science*, *13*(1), 313–342. https://doi.org/10.1146/annurev-marine-032720-095144

Perkins, S. E. (2015). A review on the scientific understanding of heatwaves—Their measurement, driving mechanisms, and changes at the global scale. *Atmospheric Research*, *164–165*, 242–267. https://doi.org/10.1016/j.atmosres.2015.05.014

Pfahl, S. (2014). Characterising the relationship between weather extremes in Europe and synoptic circulation features. *Natural Hazards and Earth System Sciences*, *14*(6), 1461–1475. https://doi.org/10.5194/nhess-14-1461-2014

Pfahl, S., & Wernli, H. (2012). Quantifying the relevance of atmospheric blocking for co-located temperature extremes in the Northern Hemisphere on (sub-)daily time scales. *Geophysical Research Letters*, *39*(12), L12807. https://doi.org/10.1029/2012GL052261

Rex, D. F. (1950). Blocking action in the middle troposphere and its effect upon regional climate. *Tellus*, 2(3), 196–211. https://doi.org/10.3402/tellusa.v2i3.8546

Riahi, K., Rao, S., Krey, V., Cho, C., Chirkov, V., Fischer, G., et al. (2011). RCP 8.5—A scenario of comparatively high greenhouse gas emissions. *Climatic Change*, *109*(1–2), 33–57. https://doi.org/10.1007/s10584-011-0149-y

Schneider, T., Bischoff, T., & Plotka, H. (2015). Physics of changes in synoptic midlatitude temperature variability. *Journal of Climate*, *28*(6), 2312–2331. https://doi.org/10.1175/JCLI-D-14-00632.1

Shaposhnikov, D., Revich, B., Bellander, T., Bedada, G., Bottai, M., Kharkova, T., et al. (2014). Mortality related to air pollution with the Moscow heat wave and wildfire of 2010. *Epidemiology*, *25*(3), 359–364. https://doi.org/10.1097/EDE.0000000000000090

Suarez-Gutierrez, L., Müller, W. A., Li, C., & Marotzke, J. (2020). Dynamical and thermodynamical drivers of variability in European summer heat extremes. *Climate Dynamics*, *54*(9–10), 4351–4366. https://doi.org/10.1007/s00382-020-05233-2

Trenberth, K. E., & Fasullo, J. T. (2012). Climate extremes and climate change: The Russian heat wave and other climate extremes of 2010. *Journal of Geophysical Research*, *117*(D17), D17103. https://doi.org/10.1029/2012JD018020

Wegren, S. K. (2011). Food security and Russia's 2010 drought. *Eurasian Geography and Economics*, *52*(1), 140–156. https://doi.org/10.2747/1539-7216.52.1.140

Woollings, T., Barriopedro, D., Methven, J., Son, S., Martius, O., Harvey, B., et al. (2018). Blocking and its response to climate change. *Current Climate Change Reports*, *4*(3), 287–300. https://doi.org/10.1007/s40641-018-0108-z

Zhao, M., Golaz, J., Held, I. M., Guo, H., Balaji, V., Benson, R., et al. (2018). The GFDL global atmosphere and land model AM4.0/LM4.0: 1. Simulation characteristics with prescribed SSTs. *Journal of Advances in Modeling Earth Systems*, *10*(3), 691–734. https://doi.org/10.1002/2017MS001208

References From the Supporting Information

Bollasina, M. A., Ming, Y., & Ramaswamy, V. (2011). Anthropogenic aerosols and the weakening of the South Asian summer monsoon. *Science*, *334*(6055), 502–505. https://doi.org/10.1126/science.1204994

Vecchi, G. A., Soden, B. J., Wittenberg, A. T., Held, I. M., Leetmaa, A., & Harrison, M. J. (2006). Weakening of tropical Pacific atmospheric circulation due to anthropogenic forcing. *Nature*, *441*(7089), 73–76. https://doi.org/10.1038/nature04744